FEATURE ARTICLE

ChemComm
www.rsc.org/chemcomm

Synthetic multifunctional pores: lessons from rigid-rod β-barrels

Naomi Sakai and Stefan Matile*
Department of Organic Chemistry, University of Geneva, Geneva, Switzerland.
E-mail: stefan.matile@chiorg.unige.ch; Fax: +41(0)22 379 3215; Tel: +41(0)22 379 6085

Received (in Cambridge, UK) 2nd April 2003, Accepted 30th June 2003
First published as an Advance Article on the web 12th August 2003

In this account, studies on synthetic multifunctional pores formed by rigid-rod β-barrels are summarized comprehensively. The first section outlines the evolution of synthetic multifunctional pores from the introduction of rigid-rod molecules in bioorganic chemistry and the discovery of synthetic β-barrels in comparison with pertinent developments in related areas of research. Design strategies to position active sites at the inner surface of rigid-rod β-barrel pores are described in the second section. The third section focuses on the characteristics of transmembrane barrel-stave pores, emphasizing the dynamic nature of supramolecular oligomers with the aid of notional phase and energy diagrams. Section four introduces multifunctionality with the use of synthetic pores as hosts of a rich collection of guests, reaching from inorganic cations to organic macromolecules like peptides, oligonucleotides, polysaccharides and polyacetylenes. In section five, practical applicability of molecular recognition by synthetic multifunctional pores is documented with non-invasive fluorometric enzyme sensing. The application of host–guest chemistry within synthetic pores to couple molecular recognition and translocation with molecular transformation is the topic of section six. The last section mentions some perspectives and challenges with synthetic multifunctional pores.

1 Introduction

The perspective to "do" chemistry within synthetic multifunctional pores (SMPs) is captivating.† Vectorial access to and spacial confinement of chemical processes that take place within the oriented "nanospace" of SMPs, on the one hand, make various modes of "remote control" envisionable. Compartmentalization by the surrounding bilayer, on the other hand, allows visualization of chemistry within SMPs with various non-trivial methods reaching from "naked eye" to single-molecule detection. In this account, we summarize the lessons learned from synthetic multifunctional pores formed by rigid-rod β-barrels (Fig. 1).[1–24] Previous reviews related to this topic emphasize barrel-stave supramolecules,[1] bioorganic chemistry of rigid-rod molecules,[2] structural[3] and functional plasticity[4] of rigid-rod β-barrels, and rigid push–pull rods.[5]

Research on synthetic multifunctional pores became possible with the discovery of synthetic routes to artificial β-barrels,[1,6] which, in turn, became accessible with the introduction of rigid-rod molecules in bioorganic chemistry.[2,25] These three hierarchical topics, *i.e.*, synthetic multifunctional pores, synthetic β-barrels, and bioorganic chemistry of rigid-rod molecules, are multiply interconnected with various areas of research. To begin with the basics, Hamilton's recent concept of *p*-oligophenyls as α-helix models is one of the few examples of rigid-rod molecules with confirmed perspectives in bioorganic chemistry.[26] Fuji's oligonaphthyl rods[27] and Strongin's more complex *p*-oligophenyls[28] hint at enormous, so far nearly unexplored, structural diversity accessible with "bioorganic" rigid rods.[29–32]

In the clearly richer world of rigid rods in supramolecular chemistry, Tilley's giant macrocycles,[30] some higher rigid-rod aromatics prepared in the groups of Müllen, Schlüter and others,[31] as well as Lehn's "skyscrapers"[32] stand out—not only because of their size. The "skyscrapers" are also leading examples of barrel-stave supramolecules built using coordination chemistry as well as of the fundamental importance of axial rigidity in refined architecture.[32]

Shifting focus from bioorganic and supramolecular rods to synthetic β-barrels, it is disturbing to note that reports on artificial (and *de-novo*) β-barrels remain rare.[1,33] This observation is even more puzzling in view of an increasingly rich collection of β-sheet secondary and quarternary[8] structures with abiotic substructures.[34] However, recent developments in amyloid research indicate that some long expected[35] shift of scientific attention from β-fibrillar quarternary structures toward tertiary β-barrel pore structures may occur in the near future.[36] Indeed, most biological pores with large interiors are β-barrels, whereas barrel-stave supramolecules formed by α-helix bundles (*i.e.*, the second pure protein tertiary structure) are usually reserved for the smaller ion channels.

Moving attention further from synthetic β-barrels to SMPs, scientific interest in the third hierarchical topic of this account appears as poor as for the previous two. However, the better recognized fields of bioengineered multifunctional pores (BMPs)‡ on the one side and synthetic ion channels and pores (SPs)§ on the other are easily identified as neighboring domains.

The internal design of biological multifunctional pores has been pioneered in the Bayley group.[37–39] Various active sites have been engineered into the ion-conducting pathway of α-hemolysin, a biological toxin, to sense cations, anionic organics,[38] host–guest complexes, oligonucleotides, proteins, and reversible covalent bond formation[39] on the single-molecule level. The perspective of single-gene sequencing within BMPs has attracted other groups to explore stochastic

Naomi Sakai (born 1964) obtained her BS from Keio University and her PhD from Tokushima Bunri University, Japan, for work on natural products under the supervision of Professor Ohfune (then at Suntory Institute of Bioorganic Research) and Professor Shizuri.

Stefan Matile (born 1963) received both Diploma and PhD from the University of Zurich, Switzerland, for contributions to the bioorganic chemistry of porphyrins studied in the group of Wolf Woggon. They met as postdocs in the group of Koji Nakanishi, Columbia University, working on visual pigments and circular dichroism (1994–1996). Since then they have worked together, first in the Department of Chemistry at Georgetown University, Washington DC (1996–1999), and then in Geneva.

DOI: 10.1039/b303649a

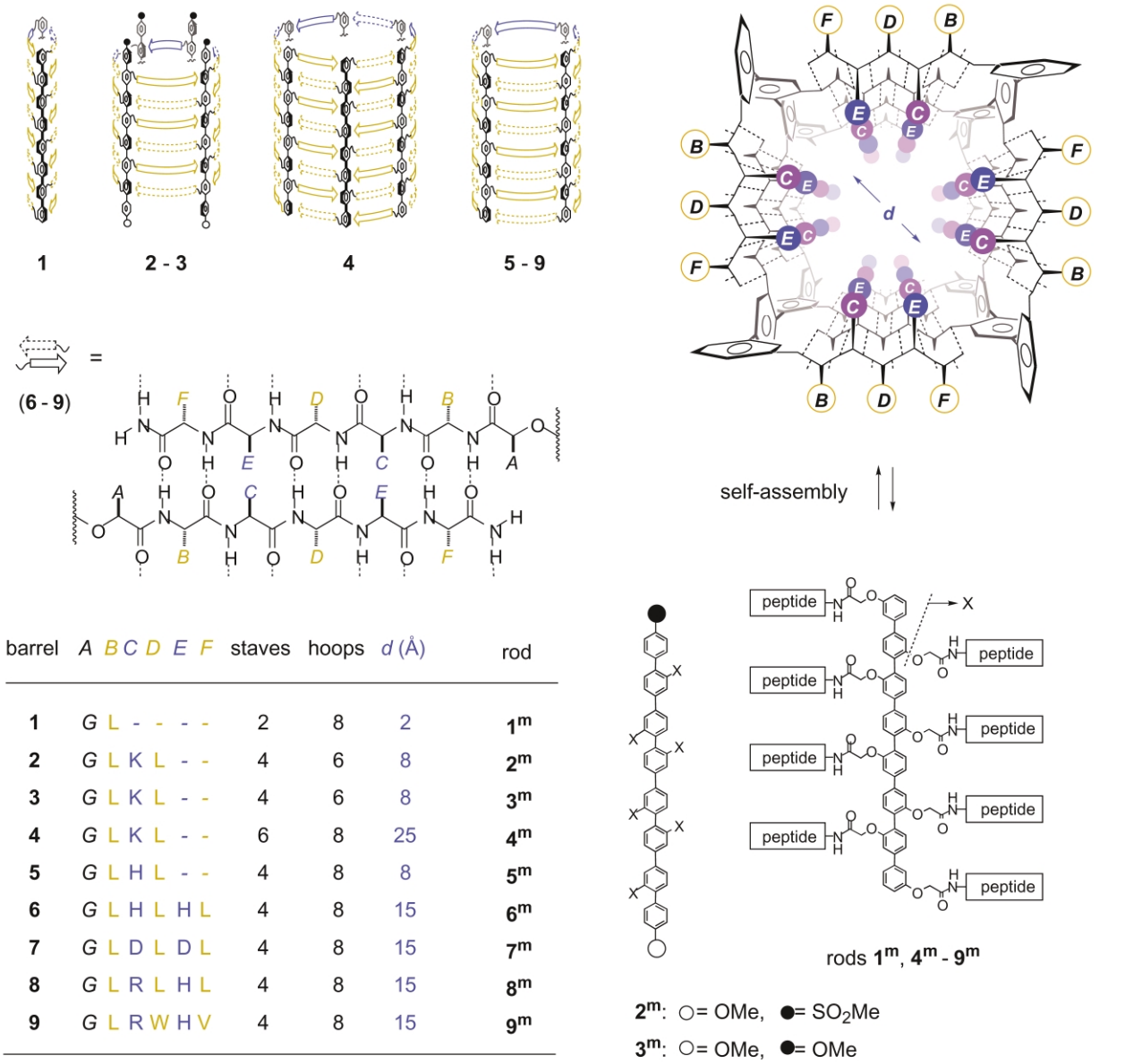

barrel	*A*	*B*	*C*	*D*	*E*	*F*	staves	hoops	*d* (Å)	rod
1	G	L	-	-	-	-	2	8	2	**1^{m}**
2	G	L	K	L	-	-	4	6	8	**2^{m}**
3	G	L	K	L	-	-	4	6	8	**3^{m}**
4	G	L	K	L	-	-	6	8	25	**4^{m}**
5	G	L	H	L	-	-	4	8	8	**5^{m}**
6	G	L	H	L	H	L	4	8	15	**6^{m}**
7	G	L	D	L	D	L	4	8	15	**7^{m}**
8	G	L	R	L	H	L	4	8	15	**8^{m}**
9	G	L	R	W	H	V	4	8	15	**9^{m}**

Fig. 1 Self-assembly of *p*-octiphenyls **1^{m}–9^{m}** into rigid-rod β-barrel pores **1–9** in blue (hydrophilic), gold (hydrophobic) and black [rigid-rod scaffolds and β-sheets, the latter as arrows or solid (backbone) and dotted lines (hydrogen bonds)]. Peptide sequences *ABCDEF* are specified separately using single-letter abbreviations (*G* = Gla = –OCH$_2$CO–, *bottom left*). Barrel stoichiometry, *i.e.*, number (*n*) of "staves" per barrel, and inner diameter *d* are implications from pore characterization (Table 1) and multifunctionality (Tables 2–5) compatible with molecular models. As in previous reports, we reiterate that the depicted suprastructures may be considered as, at worst, productive working hypotheses consistent with all experimental data available today.

sensing of oligonucleotides within the α-hemolysin β-barrel,[40,41] precedence for internal covalent capture comes from structural studies of biological pores.[42]

Many approaches to synthetic ion channels and pores (SPs)†§ have been developed over the past two decades.[1,5,43,44] Accessibility to internal design is one of the distinctive characteristics of *p*-octiphenyl β-barrels in this field.[1–24] Alternative routes to internal pore design can, however, be expected from any barrel-stave supramolecule including expanded *de-novo* α-helix bundle or "α-barrel" BMPs. Although internal design appears more challenging, the same may be true for pores formed by expanded "barrel-hoop" supramolecules (*i.e.*, stacked macrocycles) and "barrel-brick" supramolecules (*i.e.*, stacked supramolecular rosettes).[1]

As soon as chemical processes within synthetic multifunctional pores are concerned, the number and diversity of domains with scientific overlap become enormous. Evidently, molecular recognition within synthetic pores can be considered as a special case of host–guest chemistry.[26,34,45,46] Catalysis within synthetic pores may receive similarly exotic status within the fields of organic catalysis, enzyme mimicry, and enzymology.[34,46] The distinguishing characteristic of "chemistry" within SMPs, however, is that molecular recognition and transformation can be coupled with molecular translocation. Efforts toward invention and application of such "anisotropic" chemistry within the *oriented* "nanospace" of SMPs will be described in the following. The text builds up from internal pore design (section 2) to the characteristics of synthetic pores (section 3) and molecular recognition by synthetic pores (section 4) including an excursion into practical applications as enzyme sensors (section 5) to finish up with synthetic catalytic pores (section 6).

2 Internal design of multifunctional rigid-rod β-barrel pores

Rigid-rod β-barrel pores **1–9** are synthetic barrel-stave supramolecules made to exploit the seemingly limitless adaptability

of this scaffold in biology beyond pure peptide chemistry (Fig. 1). Rigid-rod β-barrels are assembled from preorganized *p*-octiphenyl "staves" **1^{m}–9^{m}**. The length of these rigid-rod staves is adjusted to roughly match the hydrophobic core of bilayer membranes composed of conventional egg yolk phosphatidylcholine. *p*-Oligophenyls are privileged rigid-rod staves because their blue emission is invaluable for structural studies in bilayer membranes and their non-planarity directs cylindrical barrel assembly. The latter process is initiated by interdigitation of the short peptide strands placed along the rigid-rod scaffold to form antiparallel β-sheets. Restricted internal space at these *p*-oligophenyl "turns" orients the first and last amino acid side chains to the outer barrel surface (Fig. 1, *B* in β_1-barrel **1**, *B* and *D* in β_3-barrels **2–5**, *B* and *F* in β_5-barrels **6–9**). β-Sheet conformation then places the neighboring amino acid residues pointing to the barrel interior (Fig. 1, *C* in β_3-barrels **2–5**, *C* and *E* in β_5-barrels **6–9**). The next residues end up again at the outer barrel surface (Fig. 1, *D* in β_5-barrels **6–9**).

Using this simple correlation between primary and tertiary peptide structure, internal and external pore design is possible by proper selection of internal residues *C* and *E* and external residues *B*, *D* and *F*, respectively. External pore design addresses pore stability and interactions with the surrounding bilayer membrane. External leucines are used routinely because an operational compromise between the β-propensity[34] and bilayer affinity[47] is reached. An extreme situation is explored in pore **9** with external valines (excellent β-propensity, miserable bilayer affinity) and tryptophans (miserable β-propensity, excellent bilayer affinity).[15] Internal design is the obvious key to "do" chemistry within synthetic multifunctional pores. β_3-Barrels with internal lysines (**2–4**) and histidines (**5**) and β_5-barrel pores with internal histidines (**6**) and aspartates (**7**) as well as histidine-arginine dyads (**8** and **9**) were synthesized for this purpose.

3 Characteristics of rigid-rod β-barrel pores

The characterization of synthetic ion channels and pores is a complex issue that continues to cause controversy. With positions reaching from superficial minimalism to preserve synthetic creativity to "fundamentalist" overemphasis of isolate methods and full-time biophysics, a reasonable balance was aimed with SMPs **1–9**, emphasizing meaningful experiments rather than accumulation of data.

Parameters of interest are summarized in Table 1 and briefly introduced in the following. A pH profile describes the dependence of pore activity on pH. For doubly pH-gated pores **4–9** with bell-shaped pH profiles, pH_{on} and pH_{off} enclose areas of maximal activity. A c_M profile describes the dependence of pore activity on monomer concentration c_M, usually at optimal pH. It can be linear ($n \approx 1$; **5–7**), increase with the *n*th power ($n > 1$; **2**, **4**, **7**, **9**), exhibit "premature" saturation ($n < 1$; **8**) or biphasic behavior (**7**). The intercept with the c_M axis (c_M^0) in $n \approx 1$ profiles may be indicative of the K_D of the pore, *n* in $n > 1$ is the average number of monomers per active pore. Fluorescence depth quenching (FDQ) differentiates between interfacial (IF), transmembrane (TM), and central (CR) location of the fluorescent "staves;" reorientations at high pore concentration or charge are given in parentheses (Fig. 2). Single-channel lifetimes τ are indicative of the stability of synthetic pores. With the exception of K-rich pores **2–4**, high stability correlated with $n \leq 1$ and poor stability with $n > 1$ in c_M profiles. Information on the inner diameter of synthetic pores comes from single-channel conductances *g*, Hille diameters d_{min}, and dye efflux. Conversion of *g* into d_{min} is worthwhile because it increases comparability by eliminating contributions from the recording solution; the intrinsic underestimate with

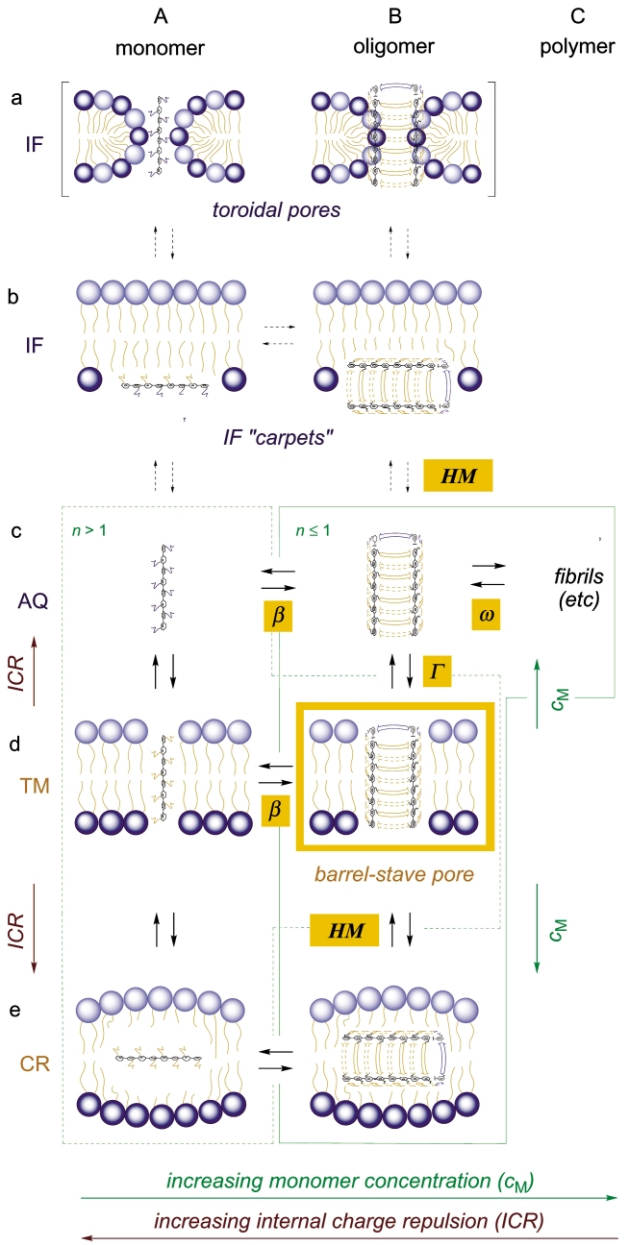

Fig. 2 Self-assembly of rigid-rod monomers (A; **1^{m}–9^{m}**) into supramolecular oligomers (B; **1–9**) and polymers (C) in aqueous bilayer suspensions (IF = interfacial, AQ = aqueous, TM = transmembrane, CR = central location). Indications include dependence on c_M (green) and *ICR*¶ (red-brown), structural implications of $n \leq 1$ (solid) and $n > 1$ (dotted) c_M profiles (green) and stabilization of TM pores **1–9** (yellow) by β-sheets (*β*), *p*-octiphenyl torsion (*ω*), partitioning (*Γ*) and hydrophobic matching (*HM*). Figs. 2–4 are highly simplified, hypothetical descriptions of supramolecular complexity involved.

Hille diameters can be visualized by efflux of organic anions of different size. Overall, long internal diameters (**6**, **7**; exception: **4**), long β-sheets (**6**, **7**, **9**; exception: **8**), and low β-propensity (**9**) contribute to pore destabilization. With hexamer **4**, pore stabilization by β-sheet truncation overrules destabilization by pore expansion. Pore **8**, in contrast, is stable despite elongated β-sheets because the inner diameter is shortened by internal counteranion immobilization ($P_{Cl^-}/P_{K^+} = 0.5$). Anion/cation selectivity complementary to internal charge characterizes pores **2**, **3**, **7** (entry 10), **8** (entry 2) and **9** (entry 12). Weakly lyotropic anion selectivity sequence implies transient anion binding with partial dehydration during translocation.[12] Deletion or inversion of ion selectivity of **7** (entry 8), **8** (entry 1) and **9** (entry 11) is attributed to immobilized internal Mg^{2+} and

inorganic phosphate, respectively. Ohmic behavior is as expected for "dipole-free" *p*-octiphenyl β-barrels. The voltage-dependent formation of pore **2**, characterized by gating charge z_g, originates from asymmetric rigid push–pull "staves." Comparable pore characteristics in planar and spherical bilayers—including ion selectivity and voltage dependence—confirms compatibility of these systems.

Taken together, these characteristics support TM rigid-rod β-barrels as active pore structures (Fig. 2Bd, yellow). They further imply that these active barrel-stave pores exist in a complex mixture of monomers (A), oligomers (B), and polymers (C) with AQ (c), TM (d) and CR (e) but not IF (a, b) location (Fig. 2, green). In general, the dynamic nature of supramolecular oligomers and polymers can not be overemphasized. For example, consistently bell-shaped pH profiles confirm that intermediate internal charge repulsion (*ICR*) is required to observe active pores.[9]¶ Linear c_M profiles with $n \approx 1$ identify stable oligomers (B) as overall relevant populations, whereas $n < 1$ profiles indicate increasing importance of supramolecular polymers (C) and $n > 1$ profiles demonstrate dominance of monomers (A).[15] Clearly, this concentration dependence of supramolecule formation hampers structural studies of active oligomers (rather than inactive monomers or polymers). Methods for "hypersensitive" and selective structure determination in bilayer membranes only can, however, bypass this limitation, at least partially. FDQ is a particularly valuable tool with *p*-octiphenyl β-barrels because the staves serve as intrinsic fluorescence labels. All pores studied by FDQ exhibited TM *p*-octiphenyl orientation at the intermediate *ICR* and c_M relevant for function (Table 1). Emergence of CR populations at elevated c_M and/or *ICR* can be explained by increasing "external" charge repulsion between aqueous (AQ) and TM populations. Consistent absence of IF populations is one of the key differences between pores formed by *p*-octiphenyl β-barrels and amphiphilic α-helix bundles.[48] The implication that *p*-octiphenyl β-barrels form true TM barrel-stave pores (Fig. 2Bd) rather than transient toroidal pores (Fig. 2a) or nondescript IF "carpets" (Fig. 2b) like many α-barrels[48] was further supported by the lack of flippase activity.[17] Even the IF preference of tryptophans[49] was overruled by the TM preference of rigid rods long enough to span the hydrophobic core of bilayer membranes (entry 11).

A summary of the above results in notional *ICR*–c_M phase diagrams may be helpful. For example, the likely origin of bell-shaped pH profiles and the four distinct c_M profiles of active oligomer pores can be visualized (Fig. 3, *ii* and *iii*). The same accounts for the importance of intermediate *ICR* and c_M to accumulate active TM oligomers and the misleading nature of structural studies of supramolecular pores at high concentration (Fig. 3*i*).

In notional energy diagrams, differentiation between excess monomer at high *ICR* and low c_M (Fig. 4, solid), excess polymer at low *ICR* and high c_M (Fig. 4, dotted) and excess oligomer at intermediate *ICR* and c_M is fundamental (Fig. 4, bold). In the context of energy diagrams, the formation of TM pores **1–9** (Fig. 2Bd) is the result of exothermic oligomerization (β), endothermic polymerization (ω), exothermic partitioning (Γ) and TM preference (*HM*, Figs. 2 and 4). From this point of view, unhindered polymerization observed with, for example, amyloid pores[35,36] is minimized by *p*-octiphenyl "turns" (ω, Figs. 2 and 4). Insufficient oligomer stabilization leading to, *e.g.*, toroidal pores with amphiphilic α-helices,[48] is minimized by β-sheet "hoops" (β, Figs. 2 and 4). The crucial importance of hydrophobic matching of rod length and bilayer thickness for TM stabilization has been verified early on using FDQ (*HM*, Figs. 2 and 4).[50–52]

Higher order aggregates of monomers **1ᵐ–9ᵐ**, *i.e.*, supramolecular rigid-rod polymers like fibrils,[8] micelles, vesicles and gels remain largely unexplored.[53] No interactions between these interesting supramolecular materials and lipid bilayer membranes have been observed.[2,50,53]

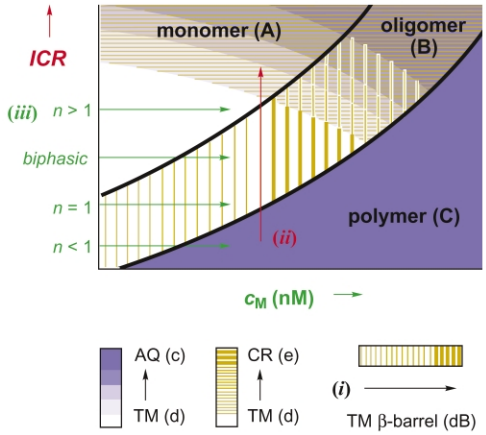

Fig. 3 Notional *ICR*–c_M phase diagram for the rigid-rod polymorphism defined in Fig. 2. (*i*) Increasing mole fraction of TM β-barrel pores, maximal at intermediate internal charge repulsion *ICR* and monomer concentration c_M. (*ii*) Origin of bell-shaped pH profiles of active oligomers (red). (*iii*) Origin of different c_M profiles (green).

4 Molecular recognition by rigid-rod β-barrel pores

The objective of internal design of synthetic pores **2–9** is to create multifunctionality. The combination of molecular translocation and molecular recognition has been explored in many variations of host, guest and method of detection (Table 2). With the exception of Mg^{2+} (**10**), studies on guest binding by pore hosts **4–9** focused on organic anions, *i.e.*, guests **11–38** (Fig. 5, Table 2). Examples reach from inorganic phosphate (**11**) to macromolecules like polypeptides (**35**, **36**), oligonucleotides (**37**, **38**), polysaccharides (**34**) and polyacetylenes (**33**). Anion binding to cation-selective pores **7** was accomplished by noncovalent conversion of apopore **7** into an anion permeable metallopore $\mathbf{7}\supset Mg^{2+}_n$ (Table 1, entries 8 and 10). Second-sphere anion inclusion within $\mathbf{7}\supset Mg^{2+}_n$ is limited, however, by the relatively high dissociation constant K_D of internal magnesium–aspartate complexes (Table 2, entry 1).

Efficient pore blockage activity was identified for pyrophosphate guests like PP, TPP, ADP and UDP as well as triphosphates like PPP and ATP. Exceptional K_D's were found for 8-R-oxy-1,3,6-pyrene trisulfonates or "cascade blues" (CBs) **25–30**. This superb molecular recognition was rationalized by topological matching of the three anions in planar CB guests and three vicinal cationic amino acid residues on one side of an antiparallel β-sheet in the pore hosts. The discovery of this novel, simple, and versatile recognition motif was crucial for the development of catalytic rigid-rod β-barrels (see section 6). Polymeric guests exhibit often nanomolar K_D's (entries 33–42). Examples of unexpectedly poor recognition could be rationalized by peripheral rather than internal guest binding, either because the pore is too small (HPTS *vs.* **5** but not **6**) or the guest is too big (heparin, perhaps also phytate).

The distinguishing characteristic of molecular recognition by SMPs is simultaneous inhibition of molecular translocation across the same SMP (Fig. 5). This interconnection opens attractive methodological and conceptual perspectives for supramolecular host–guest chemistry. For instance, adaptation of conventional dye leakage assays to pore blockage makes supramolecular host–guest chemistry visible to the "naked eye". Macroscopic pore conductance in planar bilayers is implemented as an alternative read-out for molecular recognition

Table 1 Characteristics of rigid-rod β-barrel pores[a]

Entry	pore[a] (seq)	pH profile[b] *on* ⇒ *off*	c_M profile[c] *n*	FDQ[d]	pH[e]	Stability[f] τ (ms)	Diameter[g] *g*/nS[h]	d_{min}/Å[i]	CF[j]	AD[k]	Ion selectivity P_{Cl^-}/P_{K^+}[l]	*IV* profile[m] z_g[n]	Ref.
01	**8** (LRLHL)	< 4.0 ⇒ ~ 5.5[o]	< 1[o]		6.0	> 10^3	0.3	3.3	+[o]		0.5	ohmic	14
02	**8**				4.6	> 10^3	0.3	3.3		+[o]	3.8	ohmic	14
03	**3** (LKL)			TM(CR)	7.0	> 10^3	0.9				> 1	ohmic	12
04	**2** (LKL)		> 1(4)	TM(CR)	7.0	> 10^3 ⇐ < 1	0.7				3.7	0.9 ⇒ ohmic	12
05	**4** (LKL)	~ 6.0 ⇒ > 7.5[p]	> 1(6)	TM	7.0	> 10^3	3.6		+	+[p]		ohmic	7
06	**5** (LHL)	< 4.0 ⇒ ~ 5.5[p]	~ 1[p,q]		5.0	> 10^3	0.7	5.2		+[p]		ohmic	13
07[v]	**6** (LHLHL)	< 4.0 ⇒ ~ 5.5[p]	~ 1[p,q]		5.5	35	0.3	3.1		+		ohmic	20
08	**7** ⊃ $Mg^{2+}{}_n$				6.0	12	0.3	8.8	+[r]	−[s]	0.7	ohmic	14
09	**6** (LHLHL)	< 4.0 ⇒ ~ 5.5[p]	~ 1[p,q]		5.0	5	1.2	7.0		+[p]		ohmic	20
10	**7** (LDLDL)	~ 5.5 ⇒ ~ 6.5[s]	> 1(4) ⇒ 1[s,q]	TM[t,r]	6.0	< 1	0.3	10	−[r]	+[s]	0.2	ohmic	14
11	**9** (LRWHV)	< 4.0 ⇒ ~ 5.5	> 1(4)	TM(CR)	6.0	< 1 ⇒ > 10^2			+[u]	+	0.5	ohmic	15
12	**9**				4.6	< 1				+	3.8	ohmic	15

[a] Pores are arranged in order of stability. See Fig. 1 for pores; no indication is made for unpublished material and not determined values. [b] From ANTS/DPX (AD) leakage in vesicles, *on* ⇒ *off*: activation and deactivation with increasing pH; ~: experimental data, < and >: implication. [c] Increase of activity with monomer concentration c_M; *n* ~ 1: linear above $c_M{}^0$,[q] *n* > 1: *n*th power (*n* in parentheses), *n* < 1: saturation, ⇒: biphasic. [d] Fluorescence depth quenching; TM: transmembrane, CR: central, IF: interfacial (Fig. 2); high concentration/charge effects in parentheses. [e] Concerning following data. [f] Stability according to single-channel lifetimes τ; >: approximate because of poor detectability of open/close transitions, < 1: not determined, because of short life time; ⇒: transition between short-lived and long-lived pores; dominant pore first. [g] Collection of data indicative of internal pore diameters. [h] Single-channel conductance (from linear *IV* profiles using Ohm's law). [i] Minimal inner diameter (from *g* using Hille equation; without correction). [j] Efflux of 5(6)-carboxyfluorescein. [k] Efflux of ANTS (A; 8-aminonaphthalene-1,3,6-trisulfonate) and/or DPX (D; *p*-xylenebis(pyridinium)bromide). [l] Permeability ratio (from reversal potential in *IV* profile using GHK equation; compatible with data in vesicles). [m] Dependence of activity (*e.g.*, current *I*) on voltage *V*; confirmed in vesicles. [n] Gating charge, from curve fit of non-ohmic *IV* to $\exp(z_g eV/kT)$; confirmed in vesicles. [o] From ref. 15. [p] From ref. 9. [q] Maximal c_M without detectable activity: $c_M{}^0 \approx 20$ nM. [r] From ref. 17. [s] From ref. 10. [t] Implied from absent flippase activity (Fig. 2).[17] [u] From ref. 19. [v] The origin of this low conductance level of pore **6** (entry 9) is unknown (possibilities include counterion immobilization, pore contraction, *etc.*).

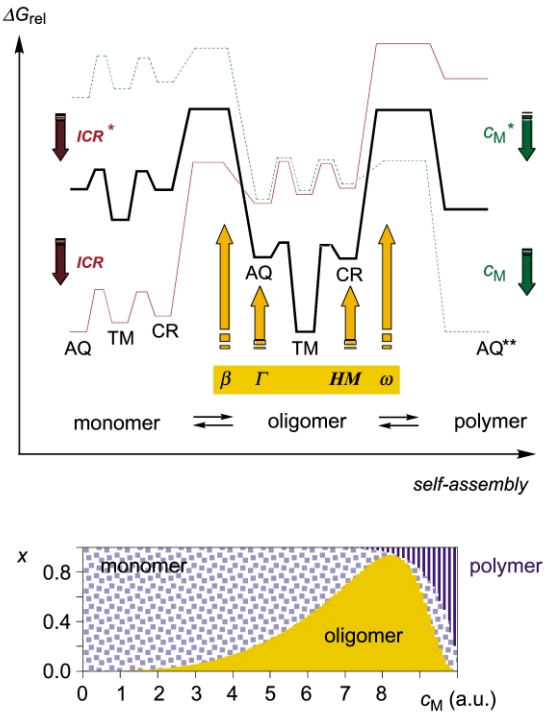

Fig. 4 *Upper:* Notional free energy diagrams for the rigid-rod polymorphism defined in Fig. 2 at low (dotted, green), intermediate (bold, black) and high *ICR* (solid, red)¶ and at low (solid, red), intermediate (bold, black) and high c_M (dotted, green). * AQ/TM/CR reorientations apply for high but not for low ICR/c_M. ** Interactions between polymers and bilayers are not considered. *Lower:* Qualitative simulation of mole fractions *x* as a function of c_M to visualize accumulation of oligomers at intermediate c_M.

within synthetic pores; improvements needed for reliable single-molecule sensing in planar bilayers justify ongoing efforts to stabilize large space within rigid-rod β-barrel SMPs.

Applications of methods in biomembrane research to structural studies include the possibility to localize molecular recognition along the ion-conducting pathway of SMP hosts from the voltage dependence of guest binding. This can help to differentiate between peripheral and internal guest binding (Table 2, entries 21*g* and 22*h*). Confirmed contributions of biomembrane characteristics to functional applications of SMPs include α-helix recognition by pore **8** in polarized membranes (Table 2, entries 36–39). This example may illustrate the attractive potential of molecular recognition within SMPs by "remote control", in this case by long-range dipole–potential interactions.

5 Detection of enzyme activity with rigid-rod β-barrel pores

Enzyme sensing is one of the practical applications of molecular recognition by SMPs (Table 3). This concept takes advantage of unique detection methods available with SMP hosts and access to a variety of substrate and product guests as exemplified in Table 2. Three distinct modes of enzyme sensing with SMPs are experimentally confirmed. Enzyme activity is monitored as pore activation if a good blocker is converted into a poor one (Fig. 6a). This is the case if the K_D of the strongest binding product exceeds the K_D of the strongest binding substrate, *i.e.*, $K_D{}^{min}(S)/K_D{}^{min}(P) < 1$. Such enzymatic pore activation was verified with apyrase, aldolase, and alkaline phosphatase (Table 3). The opposite situation, *i.e.*, pore blockage upon enzyme action with $K_D{}^{min}(S)/K_D{}^{min}(P) > 1$ (Fig. 6b), was corroborated with a glycosyltransferase. The third possibility, *i.e.*, combination of the first two situations to end up with a "pore switch" (Fig. 6c), was confirmed using galactosyltransferase to produce and alkaline phosphatase to remove pore blocker UDP.

The sensitivity of pore sensors is defined by the lowest involved $K_D{}^{min}$ (Table 3). It varies from enzyme to enzyme and from pore to pore. SMPs with internal HR dyads like **9** are consistently more sensitive than metallopore **7**⊃$Mg^{2+}{}_n$ because limitations from the millimolar K_D of internal magnesium–aspartate complexes are eliminated. The usefulness of pore **9** demonstrates that pore stability is irrelevant for enzyme sensing

Table 2 Molecular recognition by rigid-rod β-barrel pores[a]

Entry	Guest[b]				Host[a]	K_D/M[c–h]	Ref.
01	Mg^{2+}	magnesium(II)		**10**	**7** (LDLDL)	5.3×10^{-3}	17
02	P_i	inorganic phosphate	$H_nPO_4^{-(3-n)}$	**11**	**7** (LDLDL)⊃$Mg^{2+}{}_n$	6.7×10^{-2}	17
03	P_i	inorganic phosphate	$H_nPO_4^{-(3-n)}$	**11**	**9** (LRWHV)	1.2×10^{-2}	19
04	PP_i	pyrophosphate	$H_nP_2O_7^{-(4-n)}$	**12**	**7** (LDLDL)⊃$Mg^{2+}{}_n$	5.5×10^{-3}	17
05	PPP_i	triphosphate	$H_nP_3O_{10}^{-(5-n)}$	**13**	**7** (LDLDL)⊃$Mg^{2+}{}_n$	2.2×10^{-3}	17
06	TMP	thiamine monophosphate		**14**	**7** (LDLDL)⊃$Mg^{2+}{}_n$	3.0×10^{-2}	17
07	TPP	thiamine pyrophosphate		**15**	**7** (LDLDL)⊃$Mg^{2+}{}_n$	1.0×10^{-2}	17
08	TPP	thiamine pyrophosphate		**15**	**9** (LRWHV)	4.4×10^{-4}	19
09	AMP	adenosine monophosphate		**16**	**7** (LDLDL)⊃$Mg^{2+}{}_n$	2.0×10^{-2}	17
10	AMP	adenosine monophosphate		**16**	**9** (LRWHV)	6.6×10^{-5}	19
11	ADP	adenosine diphosphate		**17**	**7** (LDLDL)⊃$Mg^{2+}{}_n$	6.3×10^{-3}	17
12	ATP	adenosine triphosphate		**18**	**7** (LDLDL)⊃$Mg^{2+}{}_n$	6.7×10^{-3}	17
13	ATP	adenosine triphosphate		**18**	**9** (LRWHV)	2.0×10^{-6}	19
14	UDP	uridine diphosphate		**19**	**9** (LRWHV)	1.2×10^{-3}	19
15	G-6-P	D-glucose 6-phosphate		**20**	**7** (LDLDL)⊃$Mg^{2+}{}_n$	4.9×10^{-2}	17
16	G-1-P	α-D-glucose 1-phosphate		**21**	**7** (LDLDL)⊃$Mg^{2+}{}_n$	2.5×10^{-2}	17
17	G-1,6-DP	α-D-glucose 1,6-phosphate		**22**	**7** (LDLDL)⊃$Mg^{2+}{}_n$	1.1×10^{-2}	17
18	FDP	D-fructose 1,6-phosphate		**23**	**7** (LDLDL)⊃$Mg^{2+}{}_n$	2.2×10^{-2}	17
19	FDP	D-fructose 1,6-phosphate		**23**	**9** (LRWHV)	2.2×10^{-4}	19
20	IP_6	*myo*-inositol 1,2,3,4,5,6-hexaphosphate	phytate	**24**	**7** (LDLDL)⊃$Mg^{2+}{}_n$	3.1×10^{-2}	17
21	HPTS	8-hydroxypyrene-1,3,6-trisulfonate	(H–CB)	**25**	**5** (LHL)	1.5×10^{-3}	13[d,g]
22	HPTS	8-hydroxypyrene-1,3,6-trisulfonate	(H–CB)	**25**	**6** (LHLHL)	2.0×10^{-7}	20[d,h]
23	HPTS	8-hydroxypyrene-1,3,6-trisulfonate	(H–CB)	**25**	**8** (LRLHL)	3.0×10^{-6}	14[d]
24	HPTS	8-hydroxypyrene-1,3,6-trisulfonate	(H–CB)	**25**	**9** (LRWHV)	3.0×10^{-6}	15[d]
25	PTS	pyrene-1,3,6,8-tetrasulfonate		**26**	**6** (LHLHL)	5.0×10^{-7}	20[f]
26	PTS	pyrene-1,3,6,8-tetrasulfonate		**26**	**7** (LDLDL)⊃$Mg^{2+}{}_n$	7.1×10^{-4}	17
27	AcPTS	8-acetoxypyrene-1,3,6-trisulfonate	(C_2–CB)	**27**	**6** (LHLHL)	7.0×10^{-7}	20[e]
28	AcPTS	8-acetoxypyrene-1,3,6-trisulfonate	(C_2-CB)	**27**	**8** (LRLHL)	6.1×10^{-6}	23[e]
29	C_4–CB	8-butyryloxypyrene-1,3,6-trisulfonate	(C_4–CB)	**28**	**6** (LHLHL)	8.0×10^{-7}	20[e]
30	C_8–CB	8-octanoyloxypyrene-1,3,6-trisulfonate	(C_8–CB)	**29**	**6** (LHLHL)	1.6×10^{-6}	20[e]
31	C_{12}–CB	8-dodecanoyloxypyrene-1,3,6-trisulfonate	(C_{12}–CB)	**30**	**6** (LHLHL)	4.2×10^{-6}	20[e]
32	ANTS	8-aminonaphthalene-1,3,6-trisulfonate		**31**	**7** (LDLDL)⊃Mg^{2+}	2.9×10^{-3}	10
33		polyphosphate	$H_nP_{61}O_{184}^{-(63-n)}$	**32**	**7** (LDLDL)⊃$Mg^{2+}{}_n$	9.0×10^{-5}	17
34		poly((4-phosphonophenyl)acetylene)		**33**	**7** (LDLDL)⊃$Mg^{2+}{}_n$	8.0×10^{-6}	17
35		heparin		**34**	**7** (LDLDL)⊃$Mg^{2+}{}_n$	1.2×10^{-2}	17
36	PLGA	poly-L-glutamic acid (α-*P*-helix)	pH 4.5, $V = 0$ mV	**35**	**8** (LRLHL)	1.5×10^{-7}	18
37	PLGA	poly-L-glutamic acid (α-*P*-helix)	pH 4.5, $V \approx -150$ mV	**35**	**8** (LRLHL)	1.3×10^{-8}	18
38	PLGA	poly-L-glutamate (random coil)	pH 5.5, $V = 0$ mV	**35**	**8** (LRLHL)	4.5×10^{-8}	18
39	PLGA	poly-L-glutamate (random coil)	pH 5.5, $V \approx -150$ mV	**35**	**8** (LRLHL)	4.9×10^{-8}	18
40	PDGA	poly-D-glutamic acid (α-*M*-helix)	pH 4.5, $V = 0$ mV	**36**	**8** (LRLHL)	1.0×10^{-7}	18
41	RNA	6-FAM-rU_8-6-TAMRA		**37**	**6** (LHLHL)	n.d.	22
42	B-DNA	$d(GT)_7/d(AC)_7$		**38**	**4** (LKL)	1.8×10^{-7}	16

[a] See Fig. 1 for pores. [b] Guests not recognized under experimental conditions: Cyclic adenosine monophosphate (cAMP), imidazole and dihydroxyacetonephosphate (DHAP) by **7**⊃$Mg^{2+}{}_n$; thiamine, DHAP, uridine (U), uridine 5′-diphosphogalactose (UDPGal), uridine 5′-diphospho-*N*-acetyl-D-galactosamine, *N*-acetyl-β-D-glucosamine (GlcNAc), Galβ1 → GlcNAc, and NAcGalβ1 → GlcNAc by **9**.[17,19] [c] Dissociation constant (from Hill analysis of dose response curves for dye leakage in vesicles; exceptions: *d-f*; n.d.: not determined). [d] K_D^0 from dose response of multichannel conductance (extrapolated to $V = 0$ mV from K_D–V profiles using Woodhull equation $\log K_D = \log K_D^0 - (l_A zFV)/(2.303lRT)$). [e] K_M. [f] K_i. [g] $l_A = 0.9$ Å (distance from pores entrance to rate-limiting guest association; from K_D–V profile using Woodhull equation). [h] $l_A = 2.7$ Å.

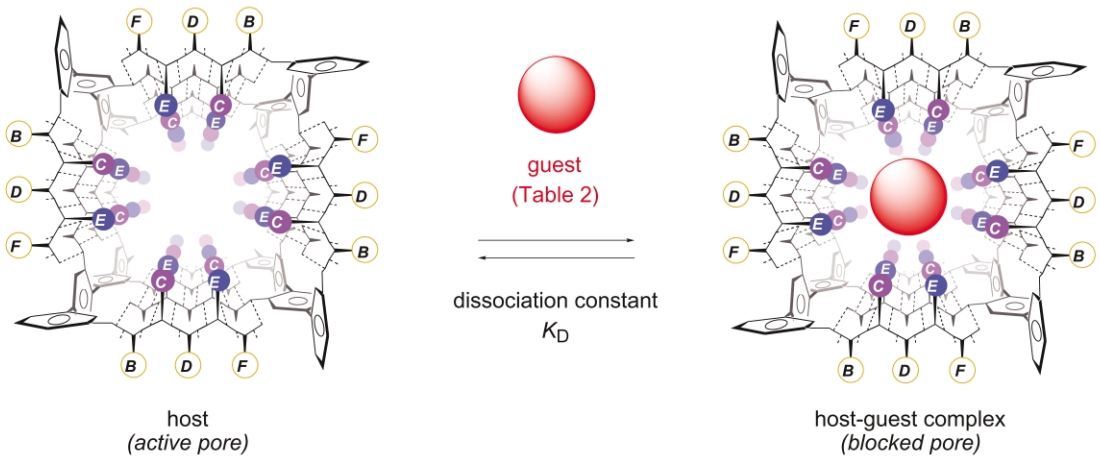

Fig. 5 Molecular recognition by synthetic multifunctional pores, depicted as simplistic universal concept; pores (Fig. 1), guests and K_D's are specified in Table 2.

Table 3 Enzymes detected with rigid-rod β-barrel pores[a]

Entry	Enzyme	Substrates (S)	Products (P)	Pore[a]	K_D^{min}/M[b]	K_D^{min}(S)/ K_D^{min}(P)[c]
01	apyrase	ATP	AMP + P_i	**7**⊃$Mg^{2+}{}_n$	6.7×10^{-3}	0.33
02	apyrase	ATP	AMP + P_i	**9**	2.0×10^{-6}	0.03
03	apyrase	ADP	AMP + P_i	**7**⊃$Mg^{2+}{}_n$	6.3×10^{-3}	0.31
04	apyrase	TPP	thiamine + P_i	**7**⊃$Mg^{2+}{}_n$	3.0×10^{-3}	0.15
05	apyrase	TPP	thiamine + P_i	**9**	4.4×10^{-4}	0.04
06	aldolase	FDP	DHAP	**7**⊃$Mg^{2+}{}_n$	2.2×10^{-2}	< 0.15
07	aldolase	FDP	DHAP	**9**	2.2×10^{-4}	< 0.09
08	alkaline phosphatase	UDP	U + P_i	**9**	1.2×10^{-3}	0.10
09	galactosyltransferase	UDPGal + GlcNAc	UDP + Galβ1 → GlcNAc	**9**	1.2×10^{-3}	> 43
10	galactosyltransferase	NAcUDPGal + GlcNAc	UDP + NAcGalβ1 → GlcNAc	**9**	1.2×10^{-3}	> 43

[a] See Fig. 1 for pores; data from ref. 19. [b] Absolute sensitivity: dissociation constant of the best pore blocker involved (compare Table 2). [c] Relative sensitivity requirement: K_D^{min} of substrate(s) divided by K_D^{min} of product(s).

(Table 1, entries 11 and 12). In clear contrast, high pore activity, preferably at low nanomolar concentrations, is crucial for evident economic reasons. Today, without an optimized format, 1 mg of pore **9** holds for more than 300 000 assays.

Compared to other assays, one key characteristic of SMPs is that the same "sensor" can be used to detect a broad variety of enzymes and substrates. This compatibility with "universal" enzyme or substrate screening is of interest with regard to practice. Moreover, SMPs sense enzymes in a non-invasive manner, *i.e.*, do not require radiolabeled or fluorogenic substrates. A third key characteristic of enzyme sensing with SMPs, *i.e.*, adaptability to various assay formats, remains unexplored beyond "naked-eye" detection using dye-loaded vesicles. Enzyme sensors with these characteristics are on demand in divers areas of scientific activity reaching from proteomics and drug discovery to "green" organic synthesis.[54,55]

6 Synthetic catalytic pores

Synthetic catalytic pores (SCPs) represent another application of molecular recognition by SMPs.† Combination of molecular translocation, recognition and transformation within SCPs yields the aesthetically pleasing and scientifically challenging situation where a substrate can enter a membrane-spanning pore on one side and appear as product on the other side of a lipid bilayer membrane. The quite straightforward detectability of currents flowing through single pores suggests that reactions that take place within SCPs could become detectable on the single-molecule level as well. Although so far not verified experimentally, the concept of single-molecule catalysis within SCPs is attractive because of the perspective to, at best, detect and characterize so far unseen reactive intermediates. Experimentally already explored is the equally thrilling application of SCPs as unique platforms to address non-trivial topics in catalysis like remote control (see below).

Apart from a study on RNase activity using FRET-labeled model oligomer **37**, synthetic catalytic pores were developed focusing on CB substrates (Table 4). Superb molecular recognition of these model substrates by SMPs (Table 2) was applied to destabilize the reactive site of hydrophilic CB substrates by remote ground-state stabilization. The use of preorganized electrostatic rather than hydrophobic interactions in this "anti-Pauling" approach[56] highlights the fundamental difference between SCPs equipped with functionalized ionic channels and classical enzyme mimics with hydrophobic binding pockets. Little dependence of CB esterolysis by pore **6** on increasing substrate hydrophobicity from CB–acetate **27** to CB–laurate **30** underscores this key characteristic of SCPs experimentally (Table 4, entries 2, 4, 5, and 6). The structural implications of such a "flat" Hansch plot are substantial and meaningful. Namely, separation of hydrophilic and hydrophobic amino acid residues in space is a unique characteristic of rigid-rod β-barrel tertiary structures that vanishes with β-barrel destruction into less organized architectures with less ordered peptide conformations including random-coil monomers.

A rich collection of data for CB esterolysis by (pre)pore **6** exists. Highlights include competitive inhibition of catalysis with PTS **26** (Table 2, entry 25) and high sensitivity toward ionic strength, pH, and barrel denaturation. The introduction of CB hydrazides as "cofactors" widens the scope of substrate diversity because otherwise unreactive, hydrophobic substrates like benzaldehyde **39** (Table 4, entry 9) become convertible as CB–hydrazone conjugates **40** (Table 4, entry 8). Compared to other esterase mimics including catalytic antibodies evolved against transition-state analogs, a ground-state stabilization by 35 kJ mol^{-1} and transition-state stabilization of 56 kJ mol^{-1} by (pre)pore **6** is quite remarkable (Table 5, entry 1). Little dependence of these characteristics on mutation of every second histidine into arginines in catalyst **8** provides corroborative evidence for the suprastructure and mode of action of supramolecular catalyst **6** (Table 5, entry 2).[23]

In bilayer membranes, the catalytic activity of β_5-barrel **6** is unchanged, whereas that of β_3-barrel **5** is further reduced. This supports that "free" CB translocation is possible through expanded pore **6** but not through contracted pore **5**. Insights on pore characteristics (Table 1, pore diameters in entries 6 and 9) and molecular recognition (Table 2, entries 21 and 22) are in support of this interpretation. Substantial multichannel pore blockage by CBs in the range of the reported K_D's—an important prerequisite for transformation during translocation—is experimentally confirmed for pores **6**, **8** and **9** (Table 2).

Preliminary studies on remote control of catalysis within the remarkably stable pore **8** (Table 1, entries 1 and 2) focus on situations that are compatible with supportive and interfering electrostatic steering. For this purpose, model substrate **27** is placed either inside or outside of spherical bilayers with inside-negative membrane potential (Fig. 7). Comparison with unpolarized membranes reveals that supportive membrane polarization guides substrates into and products out of synthetic pore **8** to overall minimize catalyst saturation. Interfering electrostatics hinder substrate access to synthetic catalytic pores as expected. Whereas elucidation of the precise origin of the potential dependence of catalysis remains to be verified, experimental evidence as such is crucial to corroborate the

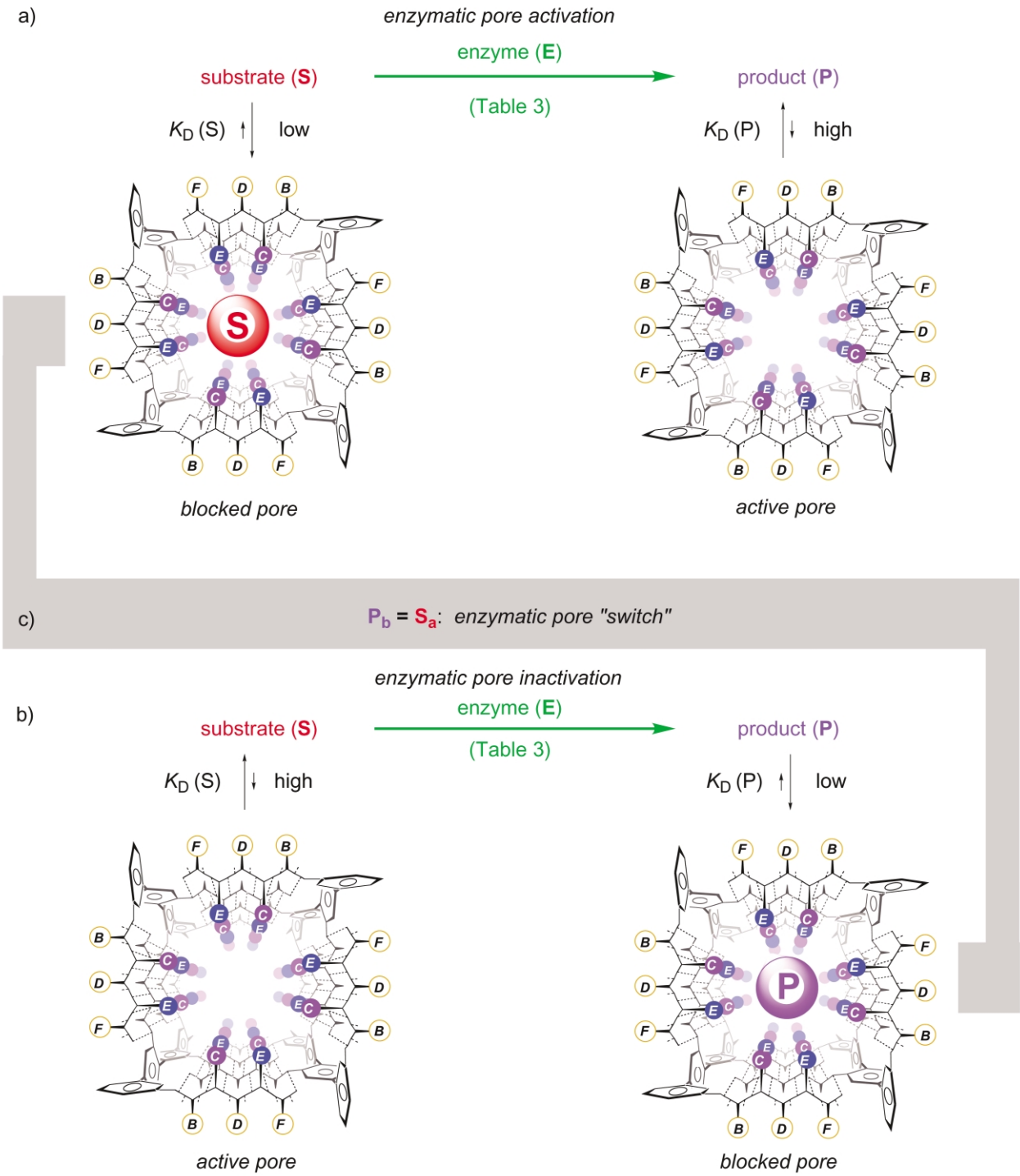

Fig. 6 Enzyme sensing with synthetic multifunctional pores, depicted schematically for a) pore activation by conversion of substrate blockers, b) pore inactivation by formation of product blockers and c) pore inactivation and activation by enzymatic formation and conversion of the same blocker.

existence of synthetic catalytic pores, *i.e.*, the possibility to couple translocation and transformation within the same pore.

7 Summary and perspectives

The bottom line is that design and synthesis of multifunctional pores is possible using the functional plasticity of rigid-rod β-barrels. One objective of this account was to sum up adventures with *p*-octiphenyl β-barrel SMPs in the hope to generate awareness for perspectives and challenges in the field. There are many. The scope and limitations of the chemical nature of rigid-rod barrel-stave supramolecules with regard to both staves other than *p*-oligophenyls and hoops other than β-sheets, for example, remain totally unexplored (discussed in section 2), not to speak of SMPs beyond barrel-stave supramolecules (discussed in the introduction). Similarly enormous diversity can be predicted for active sites positioned along the ion-conducting pathway of SMPs, their chemical nature as well as that of the complementary guests and substrates. Chemical processes that could greatly benefit from the confined and oriented "nano-space" within SMPs like templated oligomerizations or mineralizations might deserve particular attention.

There is much need to design meaningful sets of experiments to characterize synthetic multifunctional pores in a balanced manner (discussed in section 3). Implementation of optimized assay formats like high-throughput and miniaturization is

Table 4 Catalysis by rigid-rod β-barrel pores[a]

Entry	Substrates		Products		Pore[a]	Acceleration[b,c,d]	Ref.
01	**27**	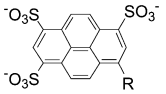 R = 	**25**	R = OH	**5** (LHL)	4.0×10^{4}[d]	13
02	**27**		**25**	R = OH	**6** (LHLHL)	9.6×10^{5}[c]	20
03	**27**		**25**	R = OH	**8** (LRLHL)	2.0×10^{5}[c]	23
04	**28**	R = 	**25**	R = OH	**6** (LHLHL)	9.0×10^{5}[c]	20
05	**29**	R = 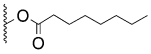	**25**	R = OH	**6** (LHLHL)	7.1×10^{5}[c]	20
06	**30**	R = 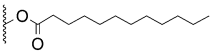	**25**	R = OH	**6** (LHLHL)	4.7×10^{5}[c]	20
07	**41**	R = 	**42**	R = NH_2	**6** (LHLHL)	1.5×10^{5}[d]	21
08[e]	**40**	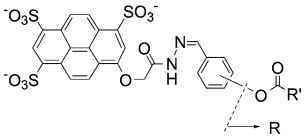	**43**	R = OH	**6** (LHLHL)	from 1.7×10^{5} to 2.3×10^{3}[d]	21
09	**39**	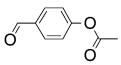	**44**		**6** (LHLHL)	1[d]	21
10	**37**	6-FAM-rU_8-6-TAMRA	**45**	6-FAM-$rU_{0–8}$	**6** (LHLHL)	3.2×10^{4}[d]	22

[a] See Fig. 1 for pores. [b] Compared to catalysis by (methyl)imidazole assuming tetrameric supramolecules and reported as [c] catalytic proficiency or [d] substrate half-life time. [e] Compare original literature for detailed structures of 12 different substrates (R, R′).

Table 5 Characteristics of rigid-rod β-barrel catalysts[a]

Entry	Pore	k_{cat}/min^{-1}	$K_M/\mu M$	$-\Delta G_{ES}^{0}$/ kJ mol^{-1}	$(k_{cat}/K_M)/k_{MeIm}$	k_{cat}/k_{uncat}	$[(k_{cat}/K_M)/k_{uncat}]/M^{-1}$	$-\Delta G_{TS}^{0}$/ kJ mol^{-1}
01	**6** (LHLHL)	0.13	0.7	35.0	9.6×10^{5}	5.0×10^{3}	7.1×10^{9}	56.0
02	**8** (LRLHL)	0.24	6.1	29.6	2.0×10^{5}	9.2×10^{3}	1.5×10^{9}	52.2

[a] See Fig. 1 for pores; substrate: 8-acetoxypyrene-1,3,6-trisulfonate (**27**); from ref. 20 and 23.

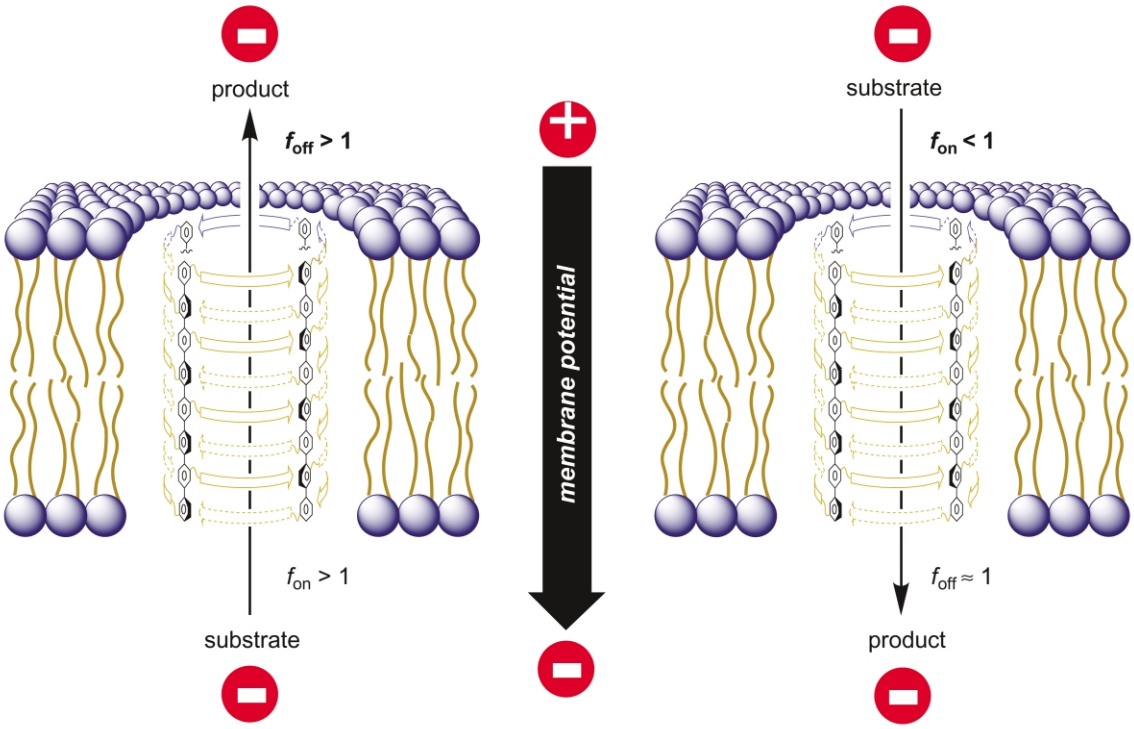

Fig. 7 Remote control (RC) of molecular transformation within synthetic catalytic pores by supportive membrane potentials accelerates substrate binding and product release (left), interference by membrane potentials decelerates substrate binding (right); f_{on} (= k_{on}^{RC}/k_{on}) and f_{off} (= k_{off}^{RC}/k_{off}). (This hypothesis is supported by preliminary results with substrate **27** and pore **8**.[23])

important for practical applications (discussed in section 5). Different to BMPs,[37–42]‡ elaboration of reliable design strategies for the construction of stable, large and transmembrane space with refined active sites remains a central challenge for single-molecule sensing within SMPs. The same accounts for the today unknown synthetic (or bioengineered) catalytic pores compatible with single-molecule detection.[13] Design strategies for active-site compression toward the middle of the SMP will be needed to maximize the effect of remote control of "chemistry within synthetic pores" (discussed in section 6). We hope that the lessons learned from rigid-rod β-barrels will encourage studies on these attractive, useful and intellectually amusing challenges with synthetic multifunctional pores.

This research has been accomplished by many productive coworkers we had the honor and the pleasure to work with. All individual contributions are acknowledged with gratitude and specified in the references. We thank the Swiss NSF (2000-064818.01 and National Research Program "Supramolecular Functional Materials" 4047-057496) for financial support.

Notes and references

† "Synthetic pores" (SPs): pores constructed from abiotic scaffolds; "synthetic multifunctional pores" (SMPs): pores constructed from abiotic scaffolds with additional function(s); "synthetic catalytic pores" (SCPs): pores constructed from abiotic scaffolds that catalyze substrate conversion *during* substrate translocation across the same pore (SPs ⊃ SMPs ⊃ SCPs).[23]

‡ "Bioengineered multifunctional pores" (BMPs):[37–42] multifunctional pores obtained by modification of biological scaffolds using biotechnological methods or synthetic organic chemistry (BMPs ≠ SMPs).

§ Herein, we differentiate synthetic channels *versus* pores with permeability for inorganics *versus* organics (pores ⊃ channels; other definitions are possible).

¶ Internal charge repulsion (*ICR*): number of charged groups at the inner surface of a pore, increases with pH for acidic residues (*e.g.*, aspartate), decreases with pH for basic residues (*e.g.*, lysine, histidine, and arginine). *ICR* model: pore activity is maximal at intermediate *ICR*.[9]

1 S. Matile, *Chem. Soc. Rev.*, 2001, **30**, 158–167.
2 S. Matile, *Chem. Rec.*, 2001, **1**, 162–172.
3 B. Baumeister, G. Das, N. Sakai and S. Matile, *Chimia*, 2001, **55**, 302–305.
4 Y. Baudry, B. Baumeister, G. Das, D. Gerard, S. Matile, N. Sakai, A. Som, N. Sordé and P. Talukdar, *Chimia*, 2002, **56**, 667–671.
5 N. Sakai and S. Matile, *Chem. Eur. J.*, 2000, **6**, 1731–1737.
6 N. Sakai, N. Majumdar and S. Matile, *J. Am. Chem. Soc.*, 1999, **121**, 4294–4295.
7 B. Baumeister, N. Sakai and S. Matile, *Angew. Chem., Int. Ed.*, 2000, **39**, 1955–1958.
8 G. Das, L. Ouali, M. Adrian, B. Baumeister, K. J. Wilkinson and S. Matile, *Angew. Chem., Int. Ed.*, 2001, **40**, 4657–4661.
9 B. Baumeister, A. Som, G. Das, N. Sakai, F. Vilbois, D. Gerard, S. P. Shahi and S. Matile, *Helv. Chim. Acta*, 2002, **85**, 2740–2753.
10 G. Das and S. Matile, *Proc. Natl. Acad. Sci. USA*, 2002, **99**, 5183–5188.
11 N. Sakai and S. Matile, *J. Am. Chem. Soc.*, 2002, **124**, 1184–1185.
12 N. Sakai, D. Houdebert and S. Matile, *Chem. Eur. J.*, 2003, **9**, 223–232.
13 A. Som, N. Sakai and S. Matile, *Bioorg. Med. Chem.*, 2003, **11**, 1363–1369.
14 N. Sakai, N. Sordé, G. Das, P. Perrottet, D. Gerard and S. Matile, *Org. Biomol. Chem.*, 2003, **1**, 1226–1231.
15 P. Talukdar, N. Sakai, N. Sordé, D. Gerard, V. M. F. Cardona and S. Matile, *Bioorg. Med. Chem.*, in press.
16 N. Sakai, B. Baumeister and S. Matile, *Chem. Bio. Chem.*, 2000, **1**, 123–125.
17 G. Das, H. Onouchi, E. Yashima, N. Sakai and S. Matile, *Chem. Bio. Chem.*, 2002, **3**, 1089–1096.
18 N. Sordé and S. Matile, *J. Supramol. Chem.*, in press.
19 G. Das, P. Talukdar and S. Matile, *Science*, 2002, **298**, 1600–1602.
20 B. Baumeister, N. Sakai and S. Matile, *Org. Lett.*, 2001, **3**, 4229–4232.
21 A. Som and S. Matile, *Eur. J. Org. Chem.*, 2002, 3874–3883.
22 B. Baumeister and S. Matile, *Macromolecules*, 2002, **35**, 1549–1555.
23 N. Sakai, N. Sordé and S. Matile, *J. Am. Chem. Soc.*, 2003, **125**, 7776–7777.
24 G. Das, N. Sakai, A. Som, N. Sordé, P. Talukdar and S. Matile, unpublished results.
25 N. Sakai, K. C. Brennan, L. A. Weiss and S. Matile, *J. Am. Chem. Soc.*, 1997, **119**, 8726–8727.
26 J. T. Ernst, O. Kutzki, A. K. Debnath, S. Jiang, H. Lu and A. D. Hamilton, *Angew. Chem., Int. Ed.*, 2002, **41**, 278–281.
27 K. Fuji, T. Furuta and K. Tanaka, *Org. Lett.*, 2001, **3**, 169–171.
28 M. W. Read, J. O. Escobedo, D. M. Willis, P. A. Beck and R. M. Strongin, *Org. Lett.*, 2000, **2**, 3201–3204.
29 P. F. H. Schwab, M. D. Levin and J. Michl, *Chem. Rev.*, 1999, **99**, 1863–1934.
30 J. R. Nitschke and T. D. Tilley, *J. Am. Chem. Soc.*, 2001, **123**, 10183–10190.
31 *Electronic Materials: The Oligomer Approach*, ed. K. Müllen and G. Wegner, Wiley-VCH, Weinheim, 1998.
32 P. N. W. Baxter, J.-M. Lehn, G. Baum and D. Fenske, *Chem. Eur. J.*, 1999, **5**, 102–112.
33 M. H. Hecht, *Proc. Natl. Acad. Sci. USA*, 1994, **91**, 8729–8730.
34 T. Sazaki and M. Lieberman, *Protein Mimetics*, in *Comprehensive Supramolecular Chemistry*, ed. Y. Murakami, Elsevier, Oxford, 1996, vol. 4, pp. 193–243.
35 S. R. Durell, H. R. Guy, N. Arispe, E. Rojas and H. B. Pollard, *Biophys. J.*, 1994, **67**, 2137–2145.
36 H. A. Lashuel, D. Hartley, B. M. Petre, T. Walz and P. T. Lansbury Jr, *Nature*, 2002, **418**, 291.
37 H. Bayley and P. S. Cremer, *Nature*, 2001, **413**, 226–230.
38 S. Cheley, L. Q. Gu and H. Bayley, *Chem. Biol.*, 2002, **9**, 829–838.
39 S. H. Shin, T. Luchian, S. Cheley, O. Braha and H. Bayley, *Angew. Chem., Int. Ed.*, 2002, **41**, 3707–3709.
40 D. W. Deamer and D. Branton, *Acc. Chem. Res.*, 2002, **35**, 817–825.
41 W. Vercoutere and M. Akeson, *Curr. Opin. Chem. Biol.*, 2002, **6**, 816–822.
42 J. A. Mindell, H. Zhan, P. D. Huynh, R. J. Collier and A. Finkelstein, *Proc. Natl. Acad. Sci. USA*, 1994, **91**, 5272–5276.
43 P. Scrimin and P. Tecilla, *Curr. Opin. Chem. Biol.*, 1999, **3**, 730–735.
44 G. W. Gokel and A. Mukhopadhyay, *Chem. Soc. Rev.*, 2001, **30**, 274–286.
45 F. P. Schmidtchen and M. Berger, *Chem. Rev.*, 1997, **97**, 1609–1646.
46 H. Dugas, *Bioorganic Chemistry*, 3rd edn., Springer, New York, USA, 1996.
47 W. C. Wimley and S. H. White, *Nature Struct. Biol.*, 1996, **3**, 842–848.
48 M. Zasloff, *Nature*, 2002, **415**, 389–395.
49 A. N. J. A. Ridder, S. Morein, J. G. Stam, A. Kuhn, B. de Kruijff and J. A. Killian, *Biochemistry*, 2000, **39**, 6521–6528.
50 B. Ghebremariam, V. Sidorov and S. Matile, *Tetrahedron Lett.*, 1999, **40**, 1445–1448.
51 C. Ni and S. Matile, *Chem. Commun.*, 1998, 755–756.
52 L. A. Weiss, N. Sakai, B. Ghebremariam, C. Ni and S. Matile, *J. Am. Chem. Soc.*, 1997, **119**, 12142–12149.
53 V. Sidorov, T. Douglas, S. M. Dzenukov, D. Abdallah, B. Ghebremariam, P. D. Roepe and S. Matile, *Chem. Commun.*, 1999, 1429–1430.
54 N. Hampp, *Science*, 2002, **298**, 1561–1562.
55 D. Wahler and J.-L. Reymond, *Curr. Opin. Chem. Biol.*, 2001, **5**, 152–158.
56 F. M. Menger, *Biochemistry*, 1992, **31**, 5368–5373.